Food Chemistry: X 24 (2024) 101992

Contents lists available at ScienceDirect

Food Chemistry: X

journal homepage: www.sciencedirect.com/journal/food-chemistry-x

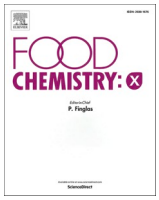

Construction of rhodamine-based fluorescent sensor for fast, on-site quantitative detection of hazardous salicylic acid in practical sample analysis

Shi-Tao Liu [a], Li-Long Zhang [a], Shuai Tan [a], Kai-Jie Wang [b], A-Ling Tang [a], Wei Niu [a], Hou-Yun Huang [a], Mei-Hong Ge [a], Lin-Lin Yang [c], Xiang Zhou [a,*], Li-Wei Liu [a], Song Yang [a,*]

[a] State Key Laboratory of Green Pesticides, Key Laboratory of Green Pesticide and Agricultural Bioengineering, Ministry of Education, Center for R&D of Fine Chemicals of Guizhou University, Guiyang 550025, China
[b] School of Chemistry and Chemical Engineering, Guizhou University, Guiyang 550025, China
[c] College of Materials Science and Engineering, Guiyang University, 550005 Guiyang, China

ARTICLE INFO

Keywords:
Fluorescent probe
Salicylic acid
Smartphone-assisted detection
Real food samples
Environmental analysis

ABSTRACT

Salicylic acid (SA) is widely used in food storage, preservatives, additives, healthcare, and the pharmaceutical industry. However, various poisoning symptoms are frequently reported upon ingestion of a large amount of SA. Therefore, discovering new tools for sensing SA with fast, simple, and portable performance is imperative. Herein, five rhodamine-based fluorescent sensors were constructed, and investigated their SA detection profiles. Probe **1** was excellent selective with a rapid response, highly sensitive (LOD = 2.5 μM), good interference resistance, and unaided eye recognition. The spray experiment and paper-based test strips indicating that probe **1** enables to the on-site and quantitatively detect SA on actual food surfaces by using a smartphone identifying the RGB values. The sensing performance was validated in soil samples, water, and various agricultural food samples. Overall, the constructed SA sensor can function as a promising, convenient, and affordable tool for point-of-care detection of SA in diversiform environmental samples.

1. Introduction

The increasing emphasis on food safety has spurred a refocusing on natural and safe antimicrobial agents to manage pathogenic microorganisms in food and postharvest fruit (Asghari & Aghdam, 2010; Koo, Heo, & Choi, 2020; J. Wang, Allan, Wang, & Yin, 2022). Salicylic acid (SA), derived from natural sources such as willow bark and other plants, has been excavated for its extensive application as a safe compound with significant potential for antimicrobial purposes in food processing and preservation (C. Chen et al., 2023; Yang, Kang, Liu, Guo, & Chen, 2022). Although SA is featured of high efficiency as a panacea for reducing human diseases and can extend the shelf life and enhance the postharvest quality of fruits and vegetables, it also leads to unknown side effects, such as urticaria, angioedema, ototoxicity, and central nervous system diseases in individuals sensitive to SA (Y. Wang et al., 2019; Q. Zhang et al., 2014). Even worse, many studies have found that SA residues pollute waterways, agricultural soil, and foods, bringing risks to human health and food safety; prolonged SA exposure can cause liver and kidney damage, dizziness, nausea, protein degeneration, and even mucosal bleeding or necrosis (Chou, Wang, Huang, & Liu, 2011; Karunanayake et al., 2017). According to European Union standards (EC1223/2009), SA in cosmetics must not exceed 0.5 %, and the Chinese Ministry of Health requires SA concentrations below 2 % in cosmetics (Cunha et al., 2023). Besides, sodium salicylate serves as a denaturant and preservative at concentrations from 0.09 % to 2 %, with concentrations of both free and bound SA, as well as free SA alone, ranging from 0 to 1 mg/kg in vegetables and fruits, and from 3 to 28 mg/kg in herbs and spices (FA Andersen, 2003; Scotter et al., 2007). Excess SA in human

Abbreviations: SA, salicylic acid; 3-OHBA, 3-hydroxybenzoic acid; MeSA, methyl salicylate; 2-MeOBA, 2-methoxybenzoic acid; 2-NH_2BA, 2-aminobenzoic acid; 4-OHBA, 4-hydroxybenzoic acid; 2-MeBA, 2-methylbenzoic acid; BA, benzoic acid; ASA, acetylsalicylic acid; 6-BA, benzylaminopurine;; 2,4-D, 2,4-dichlorophenoxyacetic acid; FQY, fluorescence quantum yield; LOD, limit of detection; DFT, density functional theory; HOMO, highest occupied molecular orbital; LUMO, lowest unoccupied molecular orbital; min, minutes; RGB, Red Green, and Blue.

* Corresponding authors.
E-mail addresses: xiangzhou@gzu.edu.cn (X. Zhou), syang@gzu.edu.cn (S. Yang).

https://doi.org/10.1016/j.fochx.2024.101992
Received 15 August 2024; Received in revised form 26 October 2024; Accepted 8 November 2024
Available online 10 November 2024
2590-1575/© 2024 Published by Elsevier Ltd. This is an open access article under the CC BY-NC-ND license (http://creativecommons.org/licenses/by-nc-nd/4.0/).

serum (>3–4 × 10^{-4} g/mL) can be toxic (Long, Chen, & Deng, 2013). So far, few methods can detect SA in fruits and vegetables. Therefore, simple and powerful methods and tools are urgently needed for quantitatively detecting SA with high sensitivity and selectivity.

The traditional technologies to detect SA include high-performance liquid chromatography-tandem mass spectrometry (HPLC-MS/MS) (Li et al., 2017), Gas chromatography-mass spectrometry (GC–MS) (Abaimov, Spavronskaya, Shabalina, Tanashyan, & Sariev, 2019), surface plasma resonance technology (Tian et al., 2012), chromatographic methods (Gruz, Ayaz, Torun, & Strnad, 2011), mass spectrometry (Pastor et al., 2012), and electrochemical analysis (Kashyap & Kumar, 2022). These methods require expensive apparatus, user expertise, pretreatment processes, low selectivity, and lengthy sample testing. To our knowledge, these methods cannot achieve facile on-site (i.e., portable) detection of SA.

To date, methods based on fluorescent probes are more favorable because of their low cost-effectiveness, simple operation, portability, and fast response (Meng et al., 2023). In particular, rhodamine-based fluorescent probes are ideal for analyte detection owing to their outstanding photophysical properties, including high molar absorption coefficient, exceptional photostability, biocompatibility, outstanding fluorescence quantum yield, and excellent water solubility (X. Chen, Pradhan, Wang, Kim, & Yoon, 2012; Zeng et al., 2023). More importantly, rhodamine probes have a robust off-on fluorescent response to analytes resulting from a switch between the non-fluorescent spirocyclic configuration and the highly fluorescent open-ring form (Muthusamy et al., 2022). Based on our previous studies of rhodamine skeleton derivatives, we envisioned obtaining a high-performance fluorescent probe by introducing optically favorable functional groups directly onto the rhodamine structure without a linker (J.-Y. Chen et al., 2023; Ma et al., 2023; Tan et al., 2024; Tang et al., 2024). Moreover, heterocyclic benzimidazole and its derivatives are helpful moieties for fluorescence detection, having unique optical properties and strong hydrogen donors (the NH group and pyridine-like nitrogen within the ring) that are useful for achieving selective binding (G. Chen, Zeng, & Huang, 2022; Molina, Tarraga, & Oton, 2012; Xiong et al., 2014). Therefore, we speculated that introducing the 2-aminobenzimidazole moiety into a rhodamine-based probe would increase the affinity and selectivity for SA in test samples.

Five rhodamine-based probes (**1–5**) were designed and synthesized as candidate SA detection probes. Probe **1**, bearing a 2-aminobenzimidazole moiety, demonstrated extreme sensitivity and selectivity toward SA, with a conspicuous fluorescence 'off-on' pattern. In this scaffold, the imidazole moiety assists in hydrogen bonding with SA, which induces electron rearrangement and the subsequent opening of the spirolactam substructure's five-membered ring. After adding SA, the color of the solution is observed by the unaided eye to change from colorless to pink, thus enabling smartphone-based capture and quantitation of test strips and food samples with a color-recognition app that extracts RGB values. To our knowledge, such a smartphone-based test strip analysis for SA detection has not been reported. To demonstrate the utility of the probe, we evaluated quantitative detection accuracy for SA in actual food samples with a routine spiking recovery study and also imaged SA in plant callus tissue. Overall, our work has produced a fast, convenient, low-cost, and reliable tool for real-time quantitative detection of SA with great potential for environmental and food safety monitoring.

2. Material and methods

2.1. Instruments and chemicals

All chemicals were obtained from Energy Chemical of Saen Chemical Technology (Shanghai) Co., Ltd., and used without further purification. HPLC/ACS-grade solvents were used for all solvents. The NMR spectra were acquired using a Bruker Biospin AG–400/500 instrument. Fluorescence spectra were recorded using a Fluoromax-4cp spectrofluorometer or PTI QuantaMaster 8000. The TU-1900 spectrophotometer recorded the ultraviolet−visible (UV − vis) spectra. UIti-Mate 3000, Thermo Scientific was employed for high-resolution mass spectrometry analysis. All experiments were repeated three times.

Probe **1** was dissolved in EtOH as the stock solution (1 mM). SA and its analogs 3-OHBA, MeSA, 2-MeOBA, phenol, 2-NH_2BA, 4-OHBA, catechol, 2-MeBA, salicylaldehyde, BA, and ASA were prepared in EtOH as a stock solution (10 mM).

2.2. Theoretical calculations of probes 1–5 with SA

The DFT computations were entirely completed by the Gaussian 16 software. All the geometry optimizations were performed via local meta-GGA exchange-correlation functional M062x with 6-31G(d) basis sets. Subsequently, frequency calculations were conducted to verify the absence of imaginary frequencies in the calculated systems. It was worth noting that all the atoms were fully relaxed in this process. The weak interactions are also taken into account by adding the relevant keyword em = GD3. Single-point calculations were conducted to obtain electronic energy using 6–311 + G(d,p) with the same function. The ethanol solvent effect was studied using the self-consistent reaction field (SCRF) approach with the SMD solvent model. Multiwfn and VMD software were employed to visualize and analyze molecular orbitals and electrostatic distributions (Humphrey, Dalke, & Schulten, 1996; Lu & Chen, 2012).

2.3. Environmental analysis

Food surface analysis experiment: Several actual food samples (cabbage, lettuce, jujube fruit, and sugar orange) were bought from the local supermarket. For example, the cabbage in the test groups was sprayed with SA solution (1 mM, 5 mM, and 10 mM), whereas the control group was pretreated with water. Then, the cabbage was air-dried to simulate the actual SA residues. Subsequently, the probe **1** solution (1 mM) was sprayed onto the surface of the cabbage. Besides, taking jujube fruit as an example, the jujube fruit in the test groups were pretreated with SA solution (spraying, 1 mM, 5 mM, and 10 mM) on their surface, while the control group underwent the treatment with water. Subsequently, these fruits were air-dried. After being immersed in the solution of probe **1** (1 mM), the test strips were subsequently tightly affixed onto the surface of the desiccated jujube fruit.

The water samples were obtained from the tap water, Yue Lake, and Huaxi River. Subsequently, the water samples were filtered through a 0.22 μm aqueous membrane and stored at room temperature. Soil samples array: Two soils (sandy and silty soil) were collected from local agricultural fields without any pretreatment. In detail, culture dishes were filled with 1 g of soil samples to obtain three groups: control, water-treated, and test groups (spraying with probe **1**). Furthermore, the water-treated group was sprayed with probe **1** solution (1 mM) for imaging. In addition, the test groups were sprayed with different SA concentrations (1 mM, 5 mM, and 10 mM, respectively) and subsequently sprayed with probe **1** solution (1 mM) on the soil surface. Finally, these photos were taken by a smartphone camera under sunlight and a UV lamp (365 nm).

2.4. Test recovery assay in different food samples

For the quantification experiment, all food samples (potato, *pachyrhizus erosus*, and white radish) were collected from the local supermarket. The samples were cut into small fragments (1 g each) and soaked in 5 mL of deionized distilled water or a certain level of SA. Subsequently, the mixtures underwent ultrasonication for 5 min, and the supernatant extracted from each sample was used as the test solution. Finally, the solution with probe **1** was added with six different concentrations of SA for the spectroscopic testing, and the spectral signal was recorded at 582 nm. Each experiment was performed in triplicate. The recovery was

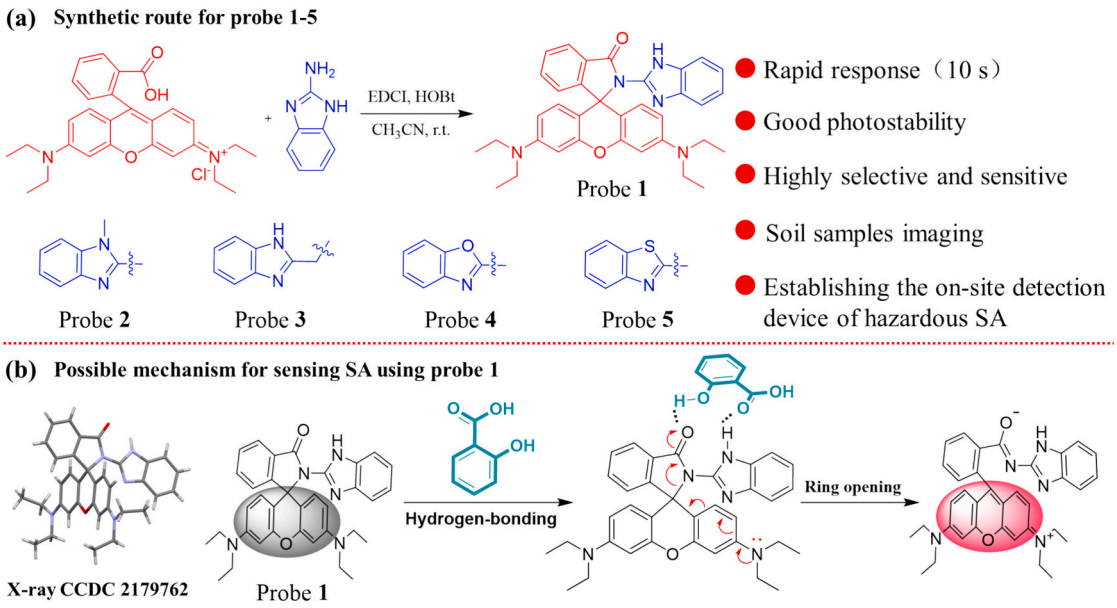

Scheme 1. (a) Synthetic routes for probe **1** to probe **5**. (b) The proposed response mechanism of probe **1** toward SA.

determined using the following equation: recovery (%) = found c / added c × 100 %. c: concentration of SA.

2.5. Detection of SA by test paper integrated with smartphone

Initially, the test paper was immersed in the solution of probe **1** (1 mM) for 1 min and air-dried at room temperature. Subsequently, the test

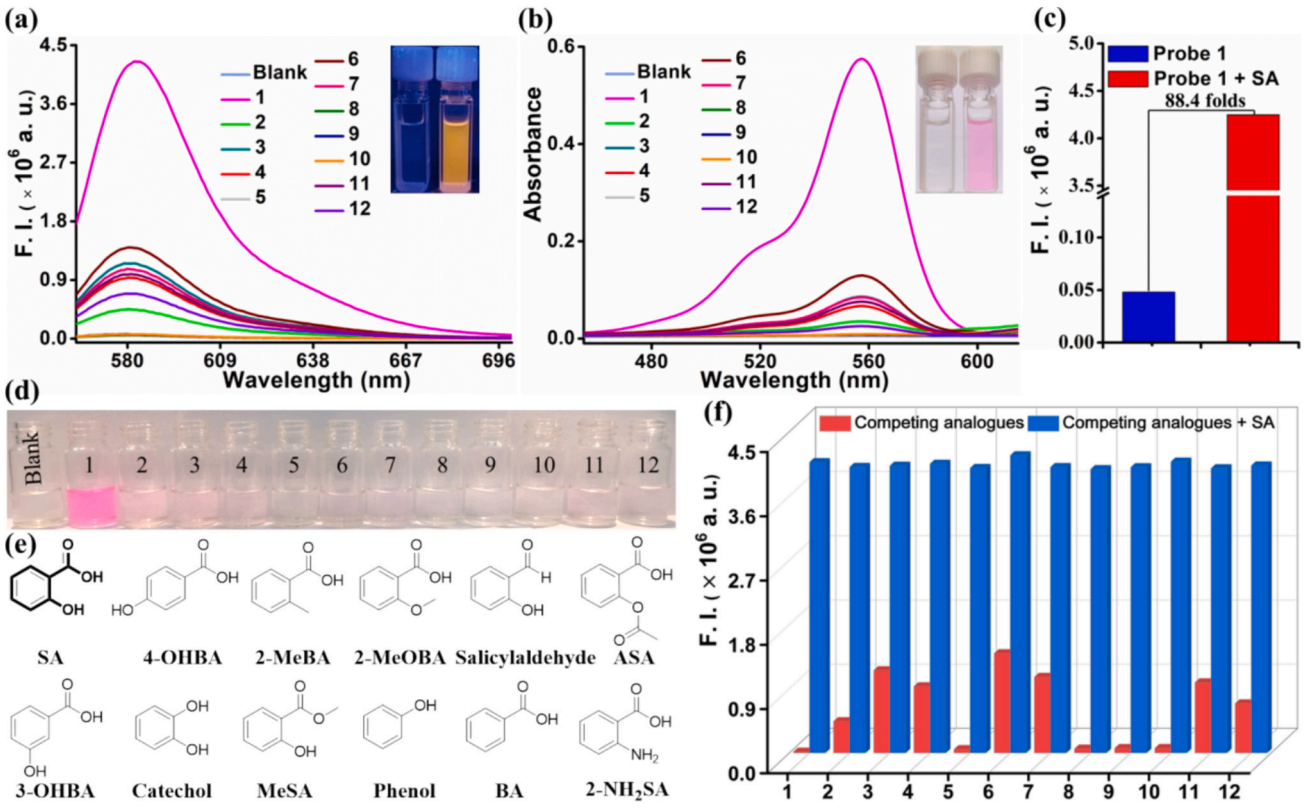

Fig. 1. (a) Fluorescence and (b) absorption spectra of probe **1** (10 μM) were recorded after the addition of SA and its analogs (50 μM) at λ_{ex} = 559 nm, using slits of 2/2 nm, and EtOH−H_2O (7:3, *v*/v) as the solvent: blank, (1) SA, (2) 4-OHBA, (3) 2-MeBA, (4) 2-MeOBA, (5) salicylaldehyde, (6) ASA, (7) 3-OHBA, (8) catechol, (9) MeSA, (10) phenol, (11) BA, and (12) 2-NH_2BA. Insert: photographs of UV light and sunlight of probe **1** in the absence or presence of SA. (c) Fluorescence enhancement ratio of the probe **1** upon the addition of SA. (d) Photographs of probe **1** (10 μM) after the addition of SA (50 μM) and its analogs. (e) The chemical structures of SA and its analogs. (f) The fluorescence intensity changes of probe **1** (10 μM) toward analogs (50 μM) at 582 nm without (red bar) or with (blue bar) 50 μM SA: (1) SA, (2) 4-OHBA, (3) 2-MeBA, (4) 2-MeOBA, (5) salicylaldehyde, (6) ASA, (7) 3-OHBA, (8) catechol, (9) MeSA, (10) phenol, (11) BA, and (12) 2-NH_2BA in EtOH-H_2O (7:3, v/v). (For interpretation of the references to color in this figure legend, the reader is referred to the web version of this article.)

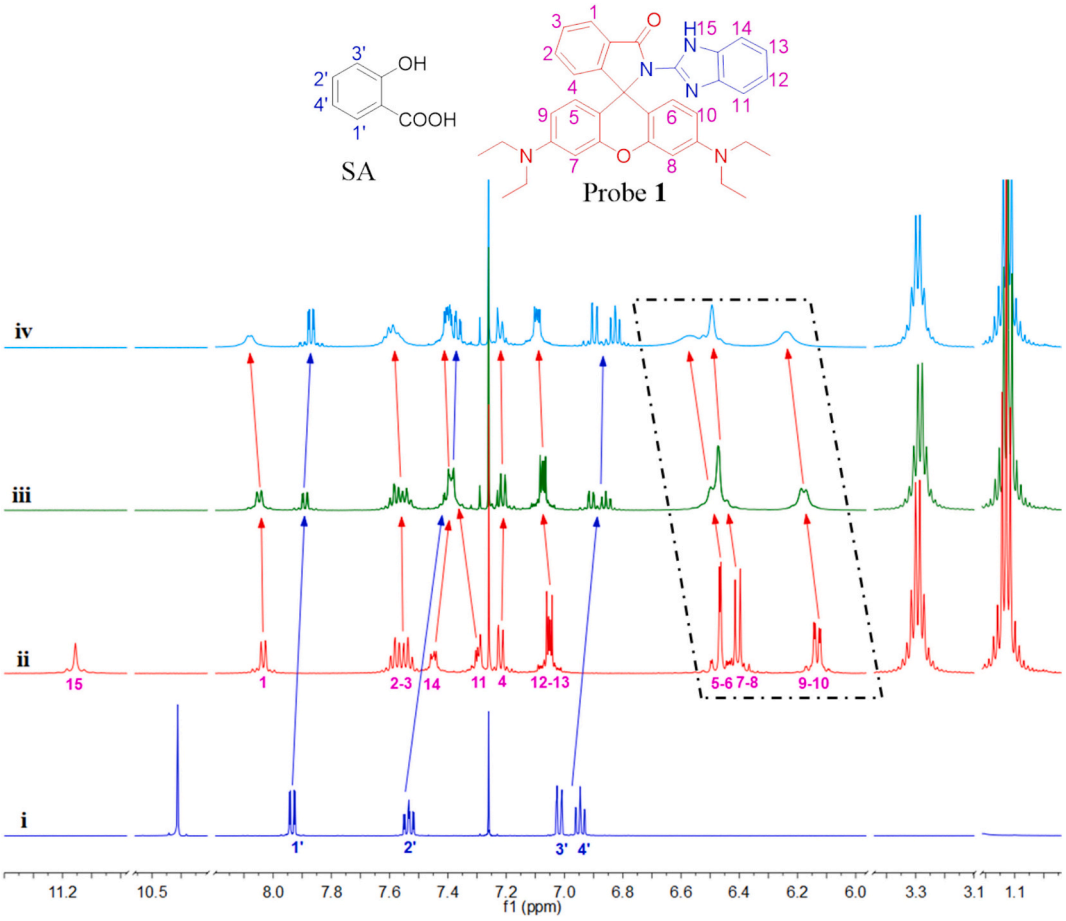

Fig. 2. ^{1}H NMR titration spectra of probe **1**, SA, and probe **1** + SA-complex with different molar ratios ((i) SA, (ii) probe **1**, (iii) probe **1**: SA = 1: 0.5, (iv) probe **1**: SA = 1: 1) in $CDCl_3$.

paper was sliced into multiple circular strips and positioned on the glass slide. Then, various concentrations of SA were dropped onto the test paper strips as treatment groups, and the water-treated sample served as the control group. Then, the liquid droplet thoroughly covered the paper surface, followed by air-drying at room temperature. In a dark environment, the fluorescence images of these paper strips were captured under a UV lamp (365 nm). Finally, the fluorescence images were directly converted as the corresponding RGB channel values for calculating the concentration of SA by establishing a linear relationship between the RGB ratio (R/B) and the concentration of SA (R/B: red channel/blue channel, c: concentration of SA).

2.6. Plant Nicotiana glutinosa L. callus culture imaging

The murashige and skoog medium containing 6-BA (0.5 mg/L), MS (5 g/L), 2,4-D (2 mg/L), and sucrose (30 g/L), were prepared to culture *Nicotiana glutinosa* L. callus. Then, probe **1** (10 μM) was added to the cell culture and incubated for various durations (2 h, 4 h, 6 h, 8 h, and 10 h), followed by washing the excess probe with sterile water three times. Subsequently, 50 μM SA was introduced into the sample for an additional 30 min. Finally, the FV30S-SW two-photon confocal fluorescence microscope recorded the SA imaging results.

3. Results and discussion

3.1. Synthesis and characterization

Five rhodamine-based fluorescent probes, **1–5**, were achieved with good yields through a straightforward one-pot reaction (Scheme 1a). The probes were elaborately characterized by using NMR, HRMS, and X-ray techniques for verifying their structures (See Fig. S1-S11 and Table S1-S6, Supporting information).

3.2. Fluorescence and absorption properties of probe 1 detecting SA

Firstly, fluorescence and UV–vis experiments were conducted to analyze the spectroscopic properties. According to the fluorescence enhancement folds at 582 nm after adding SA, the EtOH/H_2O (7:3, *v*/v) solvent system was rationally selected for the detection of SA (Fig. S12). Fig. S13 illustrated that a prominent absorption peak at 559 nm could be observed after adding SA. Correspondingly, noticeable color change (transiting the solution color from colorless to pink) can be recognized with the naked eye (see Fig. 1b). As shown in Fig. S14, there was no distinct peak in the absence of SA, which indicated that probe **1** had low background fluorescence. Upon the addition of SA, the fluorescence intensity gradually increased and reached a maximum value of 582 nm [FQY, Φ = 0.22]. Meanwhile, after adding SA, the fluorescence of the probe **1** solution rapidly transited from colorless to bright orange under exposure from a 365 nm UV lamp, indicating that probe **1**'s inherent spirolactam structure converted from its closed-loop state to its open-loop state (See Fig. 1a).

As well-known, fast detection has excellent significance in practical applications. As demonstrated in Fig. S15 and the Supporting Video S1 and Video S2, the time-dependent fluorescent spectra of the probe were investigated by triggering SA. Of note, we observed that the addition of SA did increase the fluorescence intensity and reached completion within 10 s, and a stable signal output could be maintained for more than 1 min, which demonstrates that probe **1** possesses excellent

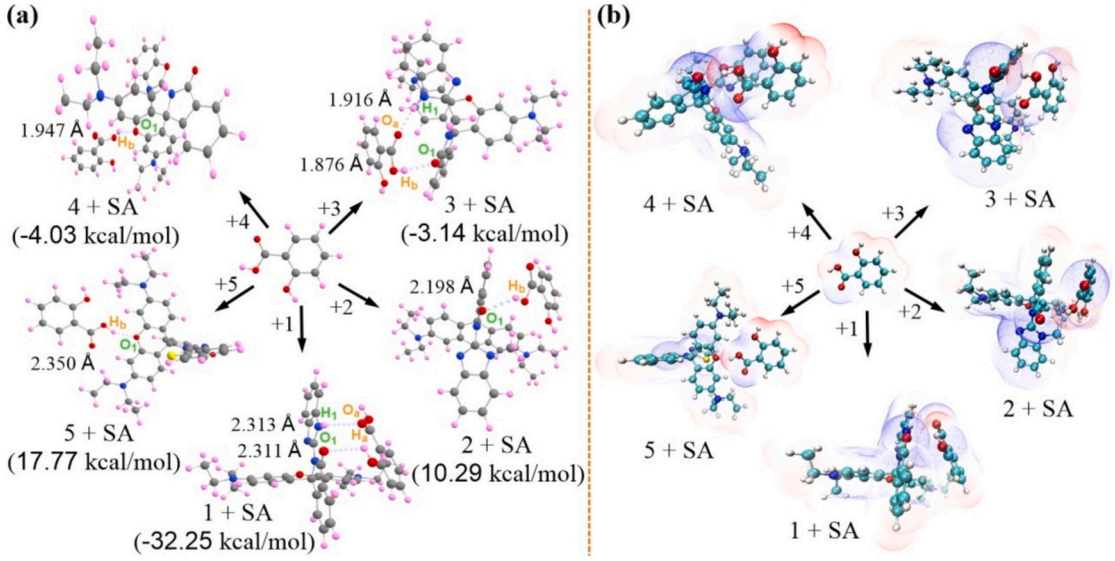

Fig. 3. (a) The optimal geometric geometry binding energy variation after adsorption of SA in probe **1**, probe **2**, probe **3**, probe **4**, and probe **5**. (b) Electrostatic potentials penetration diagram for the optimized geometries of probe **1–5** + SA.

potential for detecting SA with rapid response potency. Simultaneously, the stability of probe **1** and open loop compound **1–1** was assayed via fluorescence and UV–vis spectra, and the corresponding results were depicted in Fig. S16a-d. Interestingly, these two sensors (probe **1** and open loop compound **1–1**) maintain the constant fluorescence intensity (Fig. S16a, 16b) and UV absorption value (Fig. S16c, 16d) within 180 min, implying that they had desirable stability. Furthermore, we further investigated the spectral response of probe **1** to pH in the detection of SA. As shown in Fig. S17, the fluorescence response was inactivated within the pH range of 5–8. These results demonstrate that probe **1** possesses good stability and pH tolerance.

3.3. Selectivity and anti-interference detection of probe 1 for SA

Selectivity and anti-interference capability are two critical parameters for verifying the detection performance of the probe. UV and fluorescence selectivity of probe **1** was preferentially explored to detect SA. We evaluated the relationship between the responses of probe **1** to the relevant SA analogs (4-OHBA, 2-MeBA, 2-MeOBA, salicylaldehyde, ASA, 3-OHBA, catechol, MeSA, phenol, BA, and 2-NH_2BA). As shown in Fig. 1a, b, and Fig. 1d, compared to other SA analogs, probe **1** had superior selectivity in discerning SA from the fluorescence and absorption spectrum. The fluorescence intensities of probe **1** showed 88.4 folds significant enhancement, and the results are shown in Fig. 1c. Next, in the test system of the same condition, we also investigated the selectivity of probe **2**, probe **3**, probe **4**, and probe **5** to SA. As shown in Figs. S18 and S19, probe **2** exhibited the most considerable fluorescence enhancement for SA, and other SA analogs were following increased. Meanwhile, probe **3**, probe **4**, and probe **5** gave a very small spectral response to SA. In addition, the fluorescence intensities of probe **2**, probe **3**, probe **4**, and probe **5** showed 15.9, 12.1, 62.5, and 52.8 times significant enhancement, respectively. To sum up, the selectivity and sensitivity experiments clearly indicated that probe **1** possessed a high selectivity toward SA. Therefore, probe **1** was preferentially selected as the testing probe for SA detection in the subsequent study.

Next, anti-interference measurements of probe **1** were performed by adding interfering analogs. In detail, the interfering analogs solution was pre-treated with probe **1**, and SA solution was then added. Moreover, measurements were taken on the changes in fluorescence intensity. As depicted in Fig. 1f, none of these interfering analogs significantly affected the fluorescence intensity of probe **1**, and their fluorescence intensity hardly increased at 582 nm. These results demonstrated that probe **1** displayed a good anti-interference capability against SA.

Then, we performed the fluorescence titration experiments of probe **1** against different concentrations of SA. As expected, a notable increase in fluorescence intensity at 582 nm of probe **1** could be seen after increasing the concentration of SA. As depicted in Fig. S20, Fig. S21, and Fig. S22, the binding constant was calculated as Ka = 4.20×10^4 M^{-1}, and a good linear relationship between the probe **1** and SA (6–26 μM) concentration was obtained. The detection limit of probe **1** for SA was 2.5 μM (based on S/N = 3). Moreover, to ascertain the stoichiometry of probe **1** to SA, Job's method (Fig. S23) showed the fluorescence intensity peaked at a mole fraction of approximately 0.5, suggesting that the stoichiometry of probe **1** to SA is 1: 1.

3.4. The possible mechanism of probe 1 recognition of SA

To further rationalize the mechanisms determining the detection of SA by probe **1**, we performed the following ^{1}H NMR titration experiments. As shown in Fig. 2, Table S7 and S8, upon the addition of 0.5 and 1 equiv. of SA, the proton signals of the 1′, 2′, 3′ and 4′ of SA experience upfield shifts, while the proton signals of the 1, 2–3, 5–6, 7–8, and 9–10 of probe **1** experience downfield shifts. Alongside the prominent proton signal shift, the ^{1}H NMR titration experiments revealed a conspicuous blunting of the proton signal, which was attributed to the initiation of the ring-opening process in the spirolactam structure. With the incorporation of SA, the most significant change in ^{1}H NMR spectra was the disappearance of nitrogen hydrogen proton signal peaks in downfield shifts, indicating that the deshielding effect was triggered by the establishment of hydrogen bonds and the ring-opening of the spirolactam moiety.

For further verification of the proposed possible mechanism, the product yielded from the reaction between probe **1** and SA was separated separation on a silica gel column. As illustrated in Fig. S24 and Fig. S25, ring-opening compound **1–1** was obtained. Through meticulous analysis of the ^{1}H NMR spectra of compound **1–1**, we found that the major product was a ring-opening compound. Furthermore, we employed a high-resolution mass spectrometer to determine the molecular weight of compound **1–1**. As shown in Fig. S26, the main peak of ring-opening compound **1–1** was found at m/z = 558.2850 [M + H^+], which was consistent with the probe **1** [M + H^+]. The above results supported the proposed response mechanism (in Scheme 1b) well.

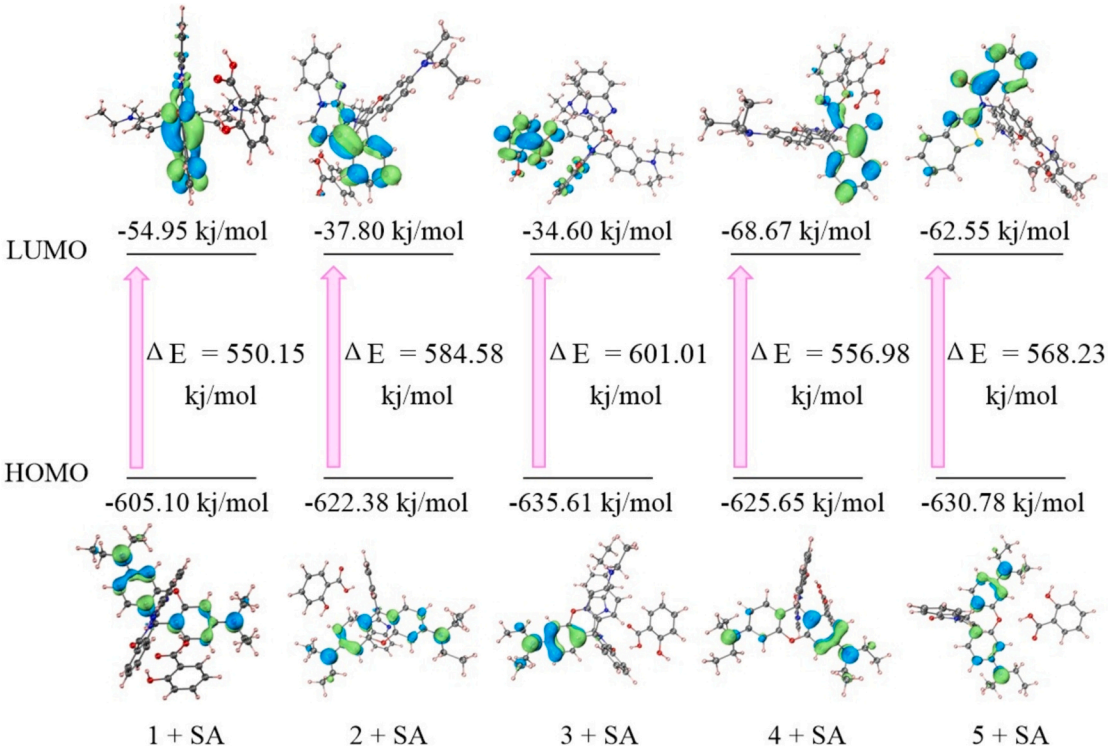

Fig. 4. (a) The HOMO–LUMO energy gap for the adsorption models of probes **1–5** and SA.

3.5. The possible SA detection mechanism of probes 1–5 by operating DFT calculations

To sufficiently identify this hypothesis binding process. Thorough investigation and elucidation were performed on the ground state geometry of the probe with SA, along with its corresponding binding energy and electronic structure. As shown in Fig. S27, DFT calculations identified that SA possessed two different configurations: stable and unstable, suggesting that the energy gaps and the configurations between the probes molecules and SA were obtained from the most energy-stable configurations. Hence, we choose SA's stable configuration for follow-up DFT studies. The binding energy (E_b) of SA and probes (**1–5**) were severally achieved and depicted in Fig. 3a and Table S9. Of note, as the excellent SA sensor, probe **1** possessed notable interaction behavior between probe and SA, two highlighted hydrogen bonds contributed to form a stable binding mode: (1) the hydrogen atom in the imidazole moiety of probe **1** could interact with the C═O group of SA, resulting in the formation of a hydrogen bond with the distance of 2.313

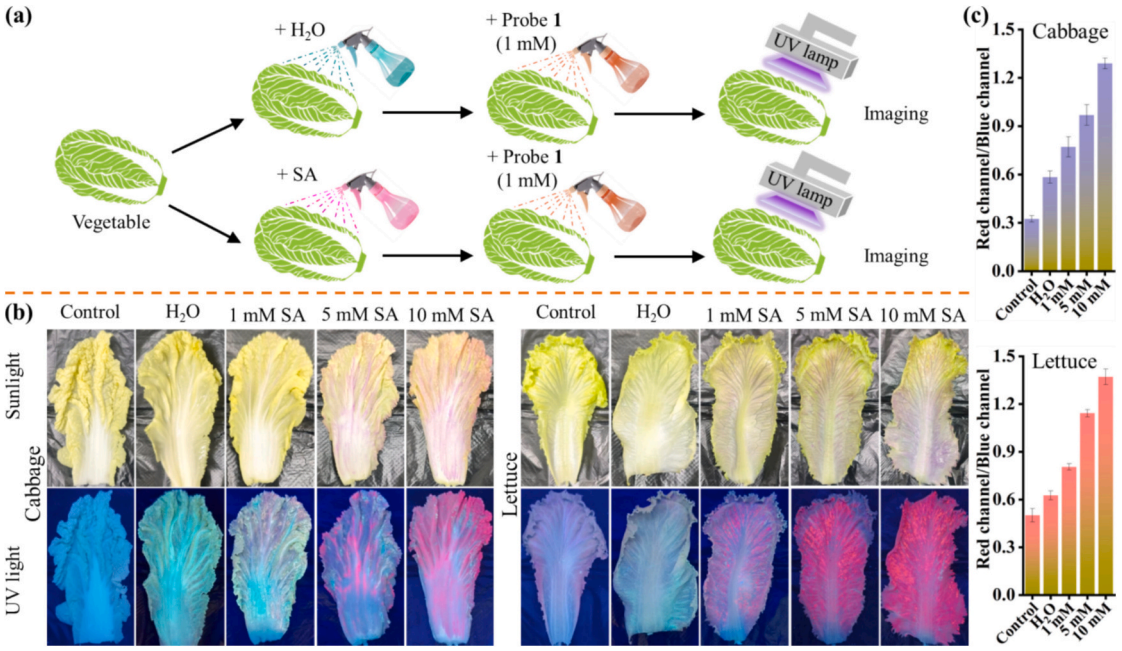

Fig. 5. (a) Depiction of imaging process for food analysis by employing probe **1** (1 mM). (b) Photographs of food samples (cabbage and lettuce) under sunlight and UV light (365 nm) with and without the presence of SA. (c) The average R/B ratios in the food samples under UV light (365 nm).

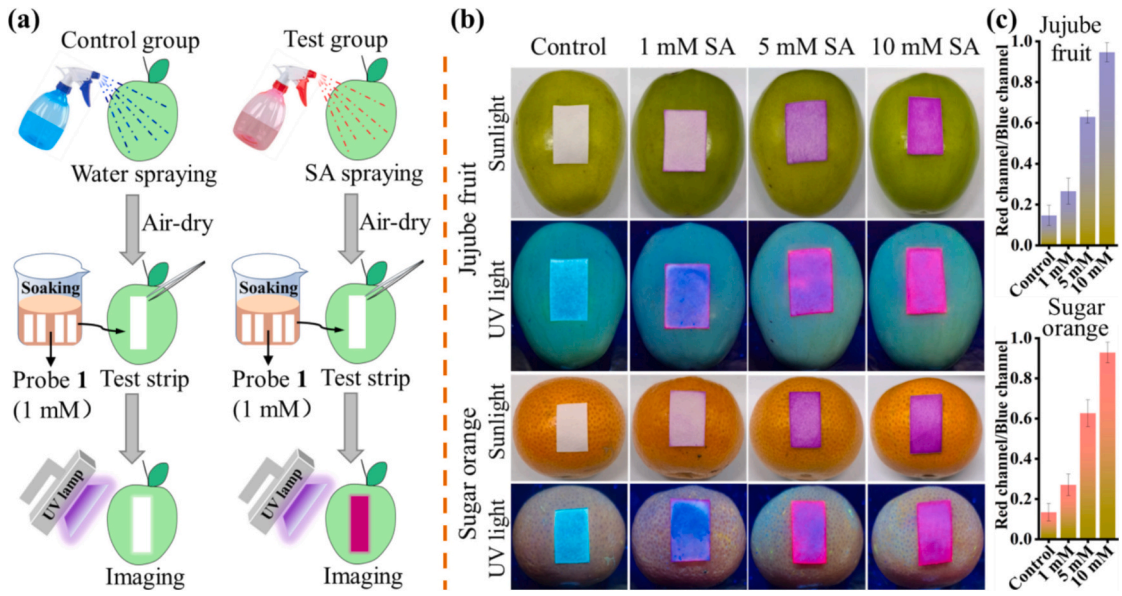

Fig. 6. (a) The procedures of detecting the paper strips in actual food analysis. (b) The photographs of the paper strips for detecting SA on jujube fruit and sugar orange were acquired and analyzed using a smartphone under sunlight and a UV lamp (365 nm). (c) The average R/B ratios of paper strips for detecting SA on jujube fruit and sugar orange under excitation light.

Å. Additionally, the C═O group of probe **1** was capable of forming another hydrogen bond with the OH group of SA, with a distance of 2.311 Å. This interesting result indicated that probe **1** might demonstrate the optimal SA sensing molecule. As was expected, the binding energy of the **1** + SA complex was −32.15 kcal/mol, which was superior to other complexes, including **2** + SA (10.29 kcal/mol), **3** + SA (−3.14 kcal/mol), **4** + SA (−4.03 kcal/mol) and **5** + SA (17.77 kcal/mol), respectively. Moreover, the electrostatic potential was further analyzed to possible the intermolecular interactions, predicting reaction sites. As displayed in Fig. 3b and Fig. S28, the electrostatic potential penetration diagram showed that SA could be primely embedded in the "off-on" recognition site of probe **1** with the comfortable electrostatic potential, thereby benefitting the optimal SA sensing performance. These meaningful findings prove that probe **1** had unprecedented sensing performance toward SA.

On the basis of the abovementioned favorable structures, the energies of the HOMO and LUMO of **1** + SA, **2** + SA, **3** + SA, **4** + SA, and **5** + SA were calculated and displayed in Fig. 4. In details, the HOMO electron charge density was mainly located on the xanthene skeleton, while the LUMO electron charge density was distributed on the substituted spironolactone ring. Meanwhile, the energy gaps are as follows: **1** + SA (550.15 kj/mol) < **4** + SA (556.98 kj/mol) < **5** + SA (568.23 kj/mol) < **2** + SA (584.58 kj/mol) < **3** + SA (601.01 kj/mol), suggesting that probe **1** was more sensitive toward SA than others. Overall, the DFT calculation results can provide meaningful and in-depth information to disclose the possible sensing mechanism and further excavate new SA sensor candidates. In addition, we proposed and depicted the possible response mechanism between probe **1** and SA in Scheme 1b.

3.6. Application of probe 1 for detecting SA in cabbage and lettuce

As a widely used preservative and antimicrobial agent, a lot of use and uptake of SA may pose side effects and potential health threats. Therefore, it is essential to detect millimole concentrations of SA in fruits and vegetables (Erdemir, Malkondu, & Oguz, 2023; M. Zhang et al., 2023). With the encouraging SA detection spectra properties results in hand, a portable, simple, and efficient spraying approach was developed for detecting SA in various actual food samples using probe **1**. The preparation and imaging process was disclosed in Fig. 5a, and specific details were provided in the experimental section (Section 2.3). As depicted in Fig. 5b, cabbage and lettuce were sprayed with SA (1 mM, 5 mM, and 10 mM), followed by the application of probe **1** solution (1 mM) on the respective food surfaces. The contrast between colorless and red can be clearly observed by the unaided eye under sunlight. Simultaneously, they promptly displayed a transition in fluorescence, shifting from cyan to red, even at a concentration of 1 mM SA, under a portable fluorescent lamp at 365 nm, demonstrating the fast and sensitive detection of SA. This study indicated that probe **1** could function as a straightforward and efficient tool for the convenient on-site detection of SA, thus safeguarding human health.

Following this, we further evaluated the applicability and practicality of probe **1** in fruit samples. Typically, millimole concentrations of SA directly impact the surface of fruits in food storage. The on-site detection ability of this method was confirmed using the as-prepared paper strips (Qin et al., 2023; Song et al., 2023). The preparation and testing procedures were disclosed in Fig. 6a, and specific details were provided in the experimental section (Section 2.3). SA (1 mM, 5 mM, and 10 mM) was sprayed on jujube fruit and sugar orange food surfaces to simulate the presence of SA residues, and then the prepared probe **1**-load (1 mM) test strips were attached to these fruit surfaces. As shown in Fig. 6b, the photographs were taken under natural sunlight and UV light (365 nm). The colorless test strips gradually changed to pink as the SA concentration increased under sunlight. Moreover, the color of the test strips transitioned from cyan fluorescence to pink fluorescence, and gradually pink deepened under UV light. This high contrast ratio color and fluorescence change could be readily observed by the unaided eye without the complicated analytical apparatus and thereby be more suitable for real-time, visual quantitative detecting of SA on food surfaces.

3.7. Fabrication of fluorescence test paper/smartphone sensor

It is widely acknowledged that a portable, simple, accurate, and quantitative device for on-site detection of SA levels will be an ideal tool for consumers (Han et al., 2024; L. Zhang, Chen, Lu, Yu, & Zhang, 2023). Keeping this belief in mind, combining the test paper's portability with the smartphone's RGB analysis function, the testing platform has been utilized for detecting SA. As shown in Fig. 7a and b, the fabrication and assay procedure of a smartphone sensing platform for SA detection was

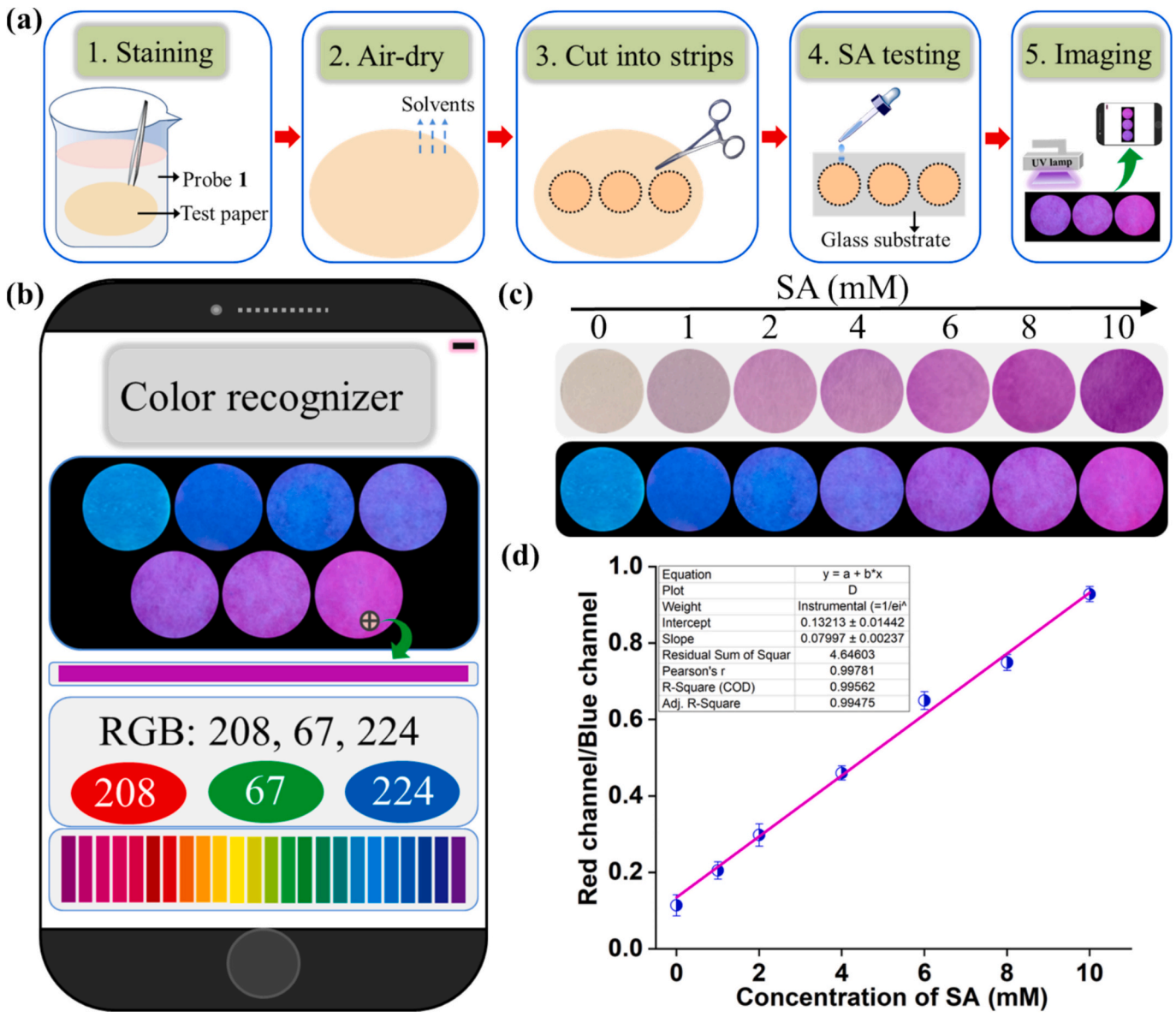

Fig. 7. (a) The procedures for the preparation and testing of the probe **1** paper strips. (b) Schematic illustration of cell phone-based signal treatment for SA quantification. (c) Photographs of the test paper (probe **1**, 1 mM) exposure to various concentrations of SA (0 mM; 1 mM; 2 mM; 4 mM; 6 mM; 8 mM; 10 mM) by using natural light with a white background and UV light (365 nm) with a black background. (d) The plot of R/B values against SA concentrations in the range of 0–10 mM.

described. As depicted in Fig. 7c, upon exposure to UV lamp (365 nm) irradiation, 1 mM concentration of probe **1** demonstrated a vibrant blue fluorescence on the test paper. In the wake of gradually increased concentrations of SA (1 mM, 2 mM, 4 mM, 6 mM, 8 mM, and 10 mM), the test paper arrays transformed from colorless to pink (exposure to natural light), and changing color from cyan to pink under UV lamp (365 nm) irradiation, which could be readily discerned with the naked eye. Fig. 7d highlighted that the R/B ratio exhibited an excellent linear correlation with SA concentrations within the 1–10 mM range, with an R^2 value of 0.99. Consequently, these findings validated the high potential of

Table 1
Determination of SA using probe **1** in various water samples.

Spiked (μM)	Tap water			River water			Lake water		
	Found (μM)	Recovery (%)	RSD (%)	Found (μM)	Recovery (%)	RSD (%)	Found (μM)	Recovery (%)	RSD (%)
0	–	–	–	–	–	–	–	–	–
6.0	6.31	105.1	1.2	6.45	107.5	1.4	6.53	108.9	2.2
10.0	9.70	97.0	3.3	9.28	92.8	4.5	9.58	95.8	1.8
14.0	13.10	93.6	1.9	14.52	103.7	2.8	14.26	101.8	4.0
18.0	17.43	96.8	3.2	17.32	96.2	4.8	18.09	100.5	2.6
22.0	21.55	97.9	2.3	21.70	98.6	1.7	20.74	94.2	3.8
26.0	26.45	101.7	2.6	24.52	94.3	2.1	25.12	96.6	4.0

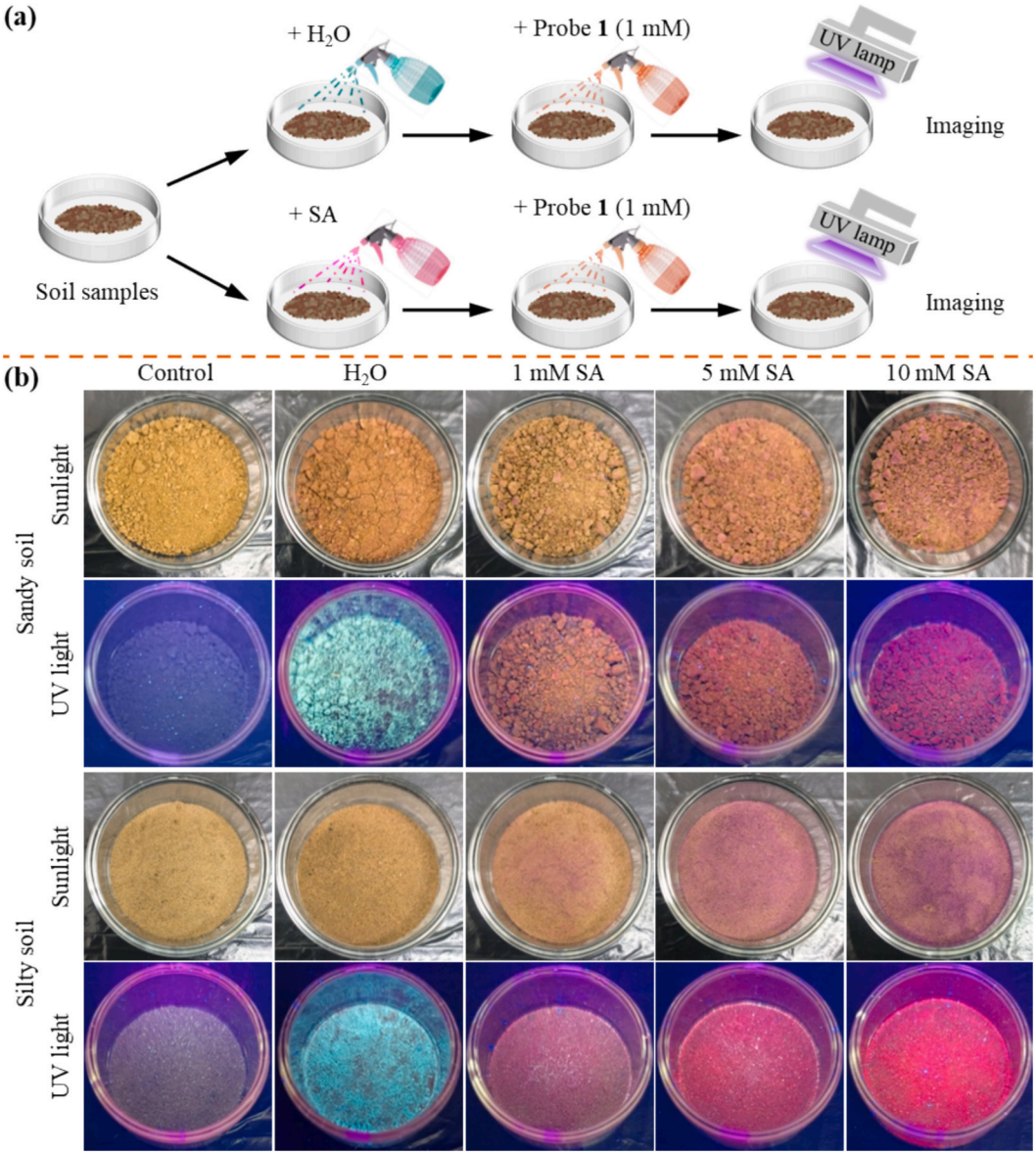

Fig. 8. (a) Schematic representation of SA detection in soil samples image using probe **1**. (b) The appearance of soil samples after spraying with SA at different concentrations (1 mM, 5 mM, and 10 mM) and then sprayed with probe **1** (1 mM). The photographs were captured by a smartphone camera under sunlight or a UV lamp (365 nm).

smartphone-assisted test paper sensor platforms for practical SA detection in daily life applications.

In order to validate the established standard linear eq. (R/B = 0.0799c + 0.1321), we conducted experiments on the surface of jujube fruit using test paper with SA concentrations, and the result is shown in Fig. S29. A smartphone color recognition software suggested the results were believable (actual concentration: 3 mM, test value 3.3 mM; actual concentration: 7 mM, test value 7.3 mM). Thus, these exciting results demonstrated that the paper-based sensing platform loading with a smartphone could be regarded as an SA detection device with precise color signals, enabling portable, accurate, rapid, and visual properties.

3.8. Environmental soil and agricultural food samples application

Given the widespread use of SA and its inadvertent release into the environment, leading to water and soil contamination, residue problems of SA potentially threaten human health and agricultural products (Dionísio et al., 2020; Lin, Sun, Yuan, & Yan, 2014). Therefore, we employed routine recovery experiments on water samples to analyze SA accurately and quantitatively. As shown in Table 1, Fig. S30, Fig. S31, and Fig. S32, three water samples (tap, lake, and river water) were analyzed using probe **1** after treatment with varying concentrations of SA. The recovery rates were gained, ranging from 92.8 % to 108.9 %, with acceptable RSD values (1.2 % ~ 4.8 %). The results indicated that probe **1** is applicable for the quantitative detection of SA in various water samples.

Next, the capability of probe **1** to detect SA in soil samples was further investigated. Fig. 8a illustrates the detailed processes of the experimental section (Section 2.3). As demonstrated in Fig. 8b, sandy and silty soil samples were sprayed with SA solution (1 mM, 5 mM, and 10 mM, respectively) and subsequently treated with probe **1** solution (1 mM) through spraying. When these samples were exposed to sunlight, the color contrast from the soil's inherent earthy yellow (control group) to red (treatment group) could be clearly observed with the naked eye. Spontaneously, the fluorescence color rapidly transitioned from cyan (0 mM SA) to red (treating with SA), gradually deepening after exposure with a portable fluorescent lamp at 365 nm and suggesting that probe **1** could be applied for the qualitative detection of SA in soil samples with

Table 2
Determination of SA spiked in various actual samples.

Spiked (μM)	Potato			*Pachyrhizus erosus*			White radish		
	Found (μM)	Recovery (%)	RSD (%)	Found (μM)	Recovery (%)	RSD (%)	Found (μM)	Recovery (%)	RSD (%)
0	–	–	–	–	–	–	–	–	–
6.0	6.43	107.3	2.0	6.87	114.6	2.7	6.73	112.3	2.4
10.0	8.80	88.0	2.2	10.22	102.2	1.8	9.33	93.3	2.8
14.0	13.77	98.4	4.4	14.05	100.3	4.4	13.90	99.3	3.3
18.0	18.45	102.5	1.2	18.08	100.4	5.3	18.06	100.3	1.0
22.0	21.54	97.9	4.6	21.04	95.6	1.6	21.91	99.6	7.1
26.0	24.06	92.5	3.0	24.55	94.4	1.4	24.20	93.0	4.5

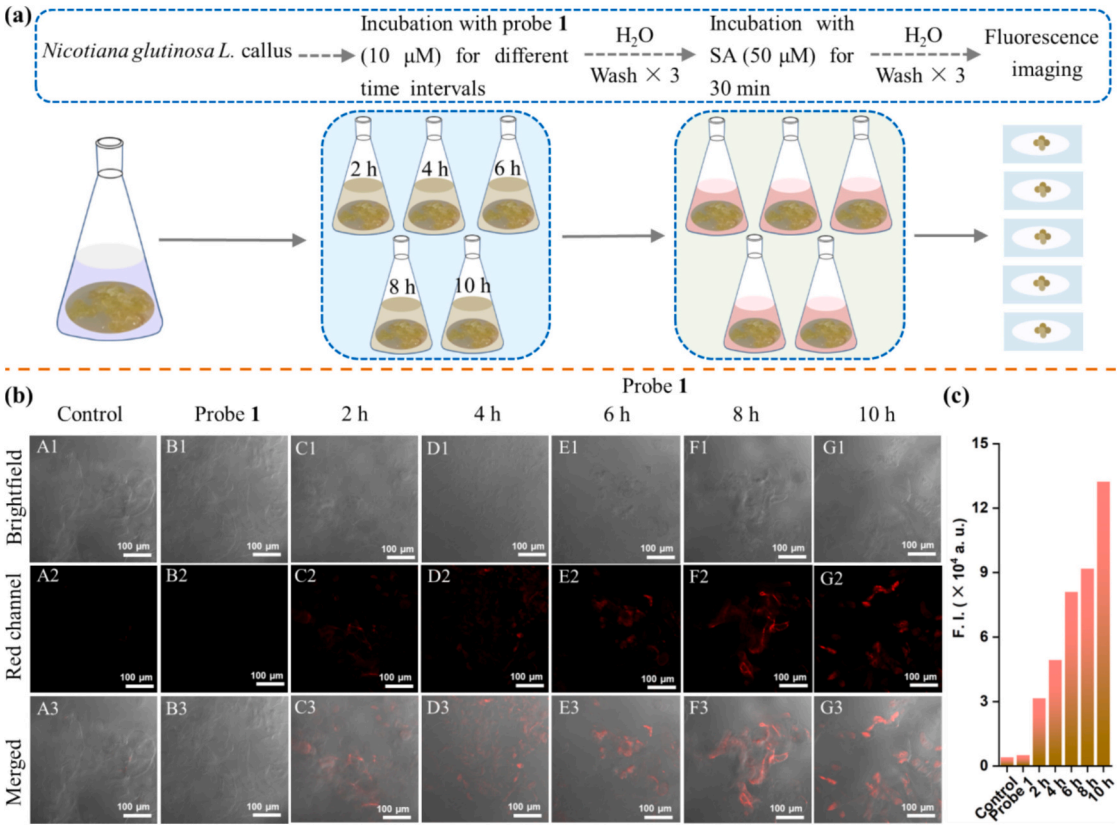

Fig. 9. (a) The incubating and treating procedure for detecting SA in *Nicotiana glutinosa* L. callus. (b) Fluorescence images of *Nicotiana glutinosa* L. callus cells incubated with probe **1** (10 μM) for 2, 4, 6, 8, and 10 h, followed by further incubation with SA (50 μM) for 30 min, showed time-dependent changes. The 1st column showed the control group, and the 2nd column showed the *Nicotiana glutinosa* L. callus cells incubated in probe **1** (10 μM) for 10 h. From top to bottom: bright field, red channel, and merged images. Scale bar: 100 μm. (c) The bar graphs depict the mean intensities of two-photon excited fluorescence in the callus. (For interpretation of the references to color in this figure legend, the reader is referred to the web version of this article.)

concentration from 1 mM to 10 mM. To the best of our knowledge, this is the first example of an SA chemical probe being used to detect SA in soil samples.

Finally, to further investigate the feasibility and accuracy of probe **1** in complex systems, we selected actual food samples such as potato, *Pachyrhizus erosus*, and white radish to assay and assess the standard recovery experiments (See Table 2, Fig. S33, Fig. S34, and Fig. S35). The recoveries in three food samples based on fluorescence detecting solution ranged from 88.0 % to 107.3 %, 94.4–114.6 %, and 93.0–112.3 %, when the SA (concentration of 6, 10, 14, 18, 22, and 26 μM) was independently introduced into the samples, and satisfactory results. These findings indicate that probe **1** is an efficient and practical tool for accurately detecting SA in actual food samples.

3.9. Fluorescence imaging of Nicotiana glutinosa L. callus

As we mentioned, environmental toxicology may lead to biological hazards, so the cell image of preliminary biological tests deserves to be assayed. Encouraged by the detection features mentioned above, the toxicity of probe **1** on A549 cells was assessed via an MTT assay. (Jiang et al., 2018, 2024; Zhang et al., 2017, 2020) As shown in Fig. S36, probe **1** exhibited no significant effect on cell viability at concentrations ranging from 10 to 60 μM, indicating low toxicity. Subsequently, we further evaluated the ability of probe **1** to detect exogenous SA in *Nicotiana glutinosa* L. callus cells via fluorescence images. The incubating and treating procedure for detecting SA is illustrated in Fig. 9a. As depicted in Fig. 9b and Fig. S37, *Nicotiana glutinosa L.* callus cells were incubated with probe **1** (10 μM) for various durations and subsequently washed three times with water as the control group (columns: B1, C4, D4, E4, and F4). Following this, the cells were incubated with SA (50 μM) for 30 min, revealing a noticeable difference in red fluorescence immediately in comparison to the control group, and the fluorescence intensity increased with time extended (rows: C2, D2, E2, F2, and G2). These results demonstrated the ability of probe **1** to respond to SA within

the cells. Over time, the intracellular uptake of probe **1** increased, facilitating the detection of exogenous SA at various intervals in the cells of plant callus tissues.

4. Conclusion

In conclusion, a series of rhodamine-based fluorescent probes were designed and synthesized. Probe 1 demonstrated excellent selectivity with a fast response time (10 s), high sensitivity (LOD = 2.5 μM), good anti-interference capability, and a color change that can be observed with the unaided eye. Interestingly, probe 1 was successfully used in spray experiments and paper-based test strips to detect SA on actual food. Significantly, a smartphone is capable of visually and quantitatively detecting SA by analyzing the RGB values of the test paper. The devised apparatus is economical, portable, and dependable for point-of-care analysis of SA in food samples. Furthermore, exogenous SA in plant callus tissue cells was distributed using probe 1, which displayed good cell permeability. Overall, this study presents a promising tool for special recognition of various concentration ranges for detecting SA residue in various food and environmental samples.

CRediT authorship contribution statement

Shi-Tao Liu: Writing – original draft, Methodology, Data curation, Conceptualization. **Li-Long Zhang:** Validation, Software, Data curation. **Shuai Tan:** Data curation. **Kai-Jie Wang:** Investigation. **A-Ling Tang:** Investigation. **Wei Niu:** Investigation. **Hou-Yun Huang:** Software. **Mei-Hong Ge:** Software. **Lin-Lin Yang:** Data curation. **Xiang Zhou:** Writing – review & editing, Investigation, Funding acquisition. **Li-Wei Liu:** Software. **Song Yang:** Writing – review & editing, Supervision, Resources, Investigation, Funding acquisition, Conceptualization.

Declaration of competing interest

The authors declare that they have no known competing financial interests or personal relationships that could have appeared to influence the work reported in this paper.

Acknowledgments

This research was financially supported by National Natural Science Foundation of China (32372610, U23A20201, 32160661, 32202359), National Key Research and Development Program of China (2022YFD1700300), and the Central Government Guides Local Science and Technology Development Fund Projects [Qiankehezhongyindi (2023) 001] and [Qiankehezhongyindi (2024) 007].

Appendix A. Supplementary data

Supplementary data to this article can be found online at https://doi.org/10.1016/j.fochx.2024.101992.

Data availability

The authors do not have permission to share data.

References

Abaimov, D. A., Spavronskaya, L. R., Shabalina, A. A., Tanashyan, M. M., & Sariev, A. K. (2019). Use of gas chromatomass spectroscopy for analysis of salicylate contents in plasma from patients with cerebrovascular diseases taking aspirin as antiaggregant therapy. *Pharmaceutical Chemistry Journal, 53*(1), 65–70. https://doi.org/10.1007/s11094-019-01957-6

Andersen, F. A. (2003). Safety assessment of salicylic acid, butyloctyl salicylate, calcium salicylate, C12-15 alkyl salicylate, capryloyl salicylic acid, hexyldodecyl salicylate, isocetyl salicylate, isodecyl salicylate, magnesium salicylate, MEA-salicylate, ethylhexyl salicylate, potassium salicylate, methyl salicylate, myristyl salicylate, sodium salicylate, TEA-salicylate, and tridecyl salicylate. *International Journal of Toxicology, 22*, 1–108. https://hero.epa.gov/hero/index.cfm/reference/details/reference_id/1098745.

Asghari, M., & Aghdam, M. S. (2010). Impact of salicylic acid on post-harvest physiology of horticultural crops. *Trends in Food Science & Technology, 21*(10), 502–509. https://doi.org/10.1016/j.tifs.2010.07.009

Chen, C., Sun, C., Wang, Y., Gong, H., Zhang, A., Yang, Y., … Li, X. (2023). The preharvest and postharvest application of salicylic acid and its derivatives on storage of fruit and vegetables: A review. *Scientia Horticulturae, 312*, 111858–111869. https://doi.org/10.1016/j.scienta.2023.111858

Chen, G., Zeng, X., & Huang, J. (2022). Imidazole-modified polymers and their adsorption of salicylic acid from aqueous solution. *Journal of Polymer Research, 29*(7), 258–264. https://doi.org/10.1007/s10965-021-02841-2

Chen, J.-Y., Tang, A.-L., Yang, P., Yang, L.-L., Tan, S., Ma, W.-J., Liu, S.-T., Huang, H.-Y., Zhou, X., Liu, L.-W., & Yang, S. (2023). Highly selective and rapid "turn-on" fluorogenic chemosensor for detection of salicylic acid in plants and food samples. *ACS Sensors, 8*(11), 4020–4030. https://doi.org/10.1021/acssensors.3c00159

Chen, X., Pradhan, T., Wang, F., Kim, J. S., & Yoon, J. (2012). Fluorescent chemosensors based on spiroring-opening of xanthenes and related derivatives. *Chemical Reviews, 112*(3), 1910–1956. https://doi.org/10.1021/cr200201z

Chou, W.-L., Wang, C.-T., Huang, K.-Y., & Liu, T.-C. (2011). Electrochemical removal of salicylic acid from aqueous solutions using aluminum electrodes. *Desalination, 271*, 55–61. https://doi.org/10.1016/j.desal.2010.12.013

Cunha, M., Silva, M. G., Marchi, L. D., Morgado, R. G., Esteves, V. I., Meucci, V., … Freitas, R. (2023). Toxic effects of a mixture of pharmaceuticals in mytilus galloprovincialis: The case of 17α-ethinylestradiol and salicylic acid. *Environmental Pollution, 324*, 121070–121082. https://doi.org/10.1016/j.envpol.2023.121070

Dionísio, R., Daniel, D., Arenas, F., Campos, J. C., Costa, P. C., Nunes, B., & Correia, A. T. (2020). Effects of pH on salicylic acid toxicity in terms of biomarkers determined in the marine gastropod *Gibbula umbilicalis*. *Marine Environmental Research, 158*, 104995–105004. https://doi.org/10.1016/j.marenvres.2020.104995

Erdemir, S., Malkondu, S., & Oguz, M. (2023). Fast, visual, and quantitative monitoring of N_2H_4 by two ratiometric fluorescent probes in environmental media and biological systems. *Chemical Engineering Journal, 468*, Article 143767. https://doi.org/10.1016/j.cej.2023.143767

Gruz, J., Ayaz, F. A., Torun, H., & Strnad, M. (2011). Phenolic acid content and radical scavenging activity of extracts from medlar (Mespilus germanica L.) fruit at different stages of ripening. *Food Chemistry, 124*(1), 271–277. https://doi.org/10.1016/j.foodchem.2010.06.030

Han, Q., Yang, M., Zhang, Z., Bai, X., Liu, X., Qin, Z., Zhang, W., Wang, P., Zhu, L., Shu, Z., & Li, X. (2024). Amine vapor-responsive ratiometric sensing tag based on HPTS/TPB-PVA fluorescent film for visual determination of fish freshness. *Food Chemistry: X, 21*, Article 101152. https://doi.org/10.1016/j.fochx.2024.101152

Humphrey, W., Dalke, A., & Schulten, K. (1996). VMD: Visual molecular dynamics. *Journal of Molecular Graphics, 14*(1), 33–38. https://doi.org/10.1016/0263-7855(96)00018-5

Jiang, Y., Huang, S., Ma, H., Weng, J., Du, X., Lin, Z., … Sun, H. (2024). RNA-activatable near-infrared photosensitizer for cancer therapy. *Journal of the American Chemical Society, 146*(36), 25270–25281. https://doi.org/10.1021/jacs.4c09470

Jiang, Y., Zheng, G., Duan, Q., Yang, L., Zhang, J., Zhang, H., … Ho, D. (2018). Ultrasensitive fluorescent probes for hypochlorite acid detection and exogenous/endogenous imaging of living cells. *Chemical Communications, 54*, 7967–7970. https://pubs.rsc.org/en/content/articlehtml/2018/cc/c8cc03963a.

Karunanayake, A. G., Todd, O. A., Crowley, M. L., Ricchetti, L. B., Pittman, C. U., Anderson, R., & Mlsna, T. E. (2017). Rapid removal of salicylic acid, 4-nitroaniline, benzoic acid and phthalic acid from wastewater using magnetized fast pyrolysis biochar from waste Douglas fir. *Chemical Engineering Journal, 319*, 75–88. https://doi.org/10.1016/j.cej.2017.02.116

Kashyap, B., & Kumar, R. (2022). A novel multi-set differential pulse voltammetry technique for improving precision in electrochemical sensing. *Biosensors and Bioelectronics, 216*, 114628–114634. https://doi.org/10.1016/j.bios.2022.114628

Koo, Y. M., Heo, A. Y., & Choi, H. W. (2020). Salicylic acid as a safe plant protector and growth regulator. *The Plant Pathology Journal, 36*(1), 1–10. https://doi.org/10.5423/PPJ.RW.12.2019.0295

Li, J.-P., Guo, J.-M., Shang, E.-X., Zhu, Z.-H., Liu, Y., Zhao, B.-C., Zhao, J., Tang, Z.-S., & Duan, J.-A. (2017). Quantitative determination of five metabolites of aspirin by UHPLC-MS/MS coupled with enzymatic reaction and its application to evaluate the effects of aspirin dosage on the metabolic profile. *Journal of Pharmaceutical and Biomedical Analysis, 138*, 109–117. https://doi.org/10.1016/j.jpba.2016.12.038

Lin, Y., Sun, X., Yuan, Q., & Yan, Y. (2014). Extending shikimate pathway for the production of muconic acid and its precursor salicylic acid in *Escherichia coli*. *Metabolic Engineering, 23*, 62–69. https://doi.org/10.1016/j.ymben.2014.02.009

Long, X., Chen, F., & Deng, M. (2013). Determination of salicylic acid in human serum and urine samples by high-performance liquid chromatography with post-column Ru $(bipy)_3^{2+}$-$Ce(SO_4)_2$ chemiluminescence detection. *Analytical Sciences, 29*(2), 227–231. https://doi.org/10.2116/analsci.29.227

Lu, T., & Chen, F. (2012). Multiwfn: A multifunctional wavefunction analyzer. *Journal of Computational Chemistry, 33*(5), 580–592. https://doi.org/10.1002/jcc.22885

Ma, W.-J., Tan, S., Yang, P., Tang, A.-L., Yang, L.-L., Chen, J.-Y., Liu, S.-T., Ge, M.-H., Zhou, X., & Yang, S. (2023). Development of benzothiazole-derived rhodamine fluorescent probes for sensitive, rapid, and reversible detection and imaging of salicylic acid in food samples and plants. *Sensors and Actuators B: Chemical, 390*, 133948–133958. https://doi.org/10.1016/j.snb.2023.133948

Meng, W.-Q., Sedgwick, A. C., Kwon, N., Sun, M., Xiao, K., He, X.-P., … Yoon, J. (2023). Fluorescent probes for the detection of chemical warfare agents. *Chemical Society Reviews, 52*(2), 601–662. https://doi.org/10.1039/D2CS00650B

Molina, P., Tarraga, A., & Oton, F. (2012). Imidazole derivatives: A comprehensive survey of their recognition properties. *Organic & Biomolecular Chemistry, 10*(9), 1711–1724. https://doi.org/10.1039/C2OB06808G

Muthusamy, S., Rajalakshmi, K., Kannan, P., Zhu, D., Seo, Y., Zhu, W., … Nam, Y.-S. (2022). Targeting citrate as novel strategy in diagnosing prostate cancer using rhodamine extended red emissive fluorophore: Sensing mechanism and prostate tumor diagnosis applications. *Sensors and Actuators B: Chemical, 369*, 132299–132309. https://doi.org/10.1016/j.snb.2022.132299

Pastor, V., Vicent, C., Cerezo, M., Mauch-Mani, B., Dean, J., & Flors, V. (2012). Detection, characterization and quantification of salicylic acid conjugates in plant extracts by ESI tandem mass spectrometric techniques. *Plant Physiology and Biochemistry, 53*, 19–26. https://doi.org/10.1016/j.plaphy.2012.01.003

Qin, T., Zhao, X., Song, C., Lv, T., Chen, S., Xun, Z., Xu, Z., Zhang, Z., Xu, H., Zhao, C., Liu, B., & Peng, X. (2023). A ratiometric supramolecular fluorescent probe for on-site determination of cyfluthrin in real food samples. *Chemical Engineering Journal, 451*, Article 139022. https://doi.org/10.1016/j.cej.2022.139022

Scotter, M. J., Roberts, D. P. T., Wilson, L. A., Howard, F. A. C., Davis, J., & Mansell, N. (2007). Free salicylic acid and acetyl salicylic acid content of foods using gas chromatography–mass spectrometry. *Food Chemistry, 105*(1), 273–279. https://doi.org/10.1016/j.foodchem.2007.03.007

Song, C., Zeng, C., Qin, T., Lv, T., Xu, Z., Xun, Z., Wang, L., Chen, X., Liu, B., & Peng, X. (2023). A dual-state-emission chalcone-based supramolecular probe for ratiometric detection of penconazole in environmental samples. *Chemical Engineering Journal, 468*, Article 143610. https://doi.org/10.1016/j.cej.2023.143610

Tan, S., Tang, A.-L., Niu, W., Wang, G.-Y., Gao, F., Yang, P., Liu, S.-T., Yang, L.-L., Liu, L.-W., Zhou, X., & Yang, S. (2024). Engineering a ratiometric fluorescent sensor-based tool for detection of phytohormone salicylic acid and its application in physiological and pathological processes. *Sensors and Actuators B: Chemical, 420*, Article 136416. https://doi.org/10.1016/j.snb.2024.136416

Tang, A.-L., Zhang, L.-L., Tan, S., Yang, P., Niu, W., Ge, M.-H., Yang, L.-L., Wang, P.-Y., Liu, L.-W., Zhou, X., & Yang, S. (2024). Host-guest synergistic hydrogen bond triggered signal amplification for visualizing the plant hormone salicylic acid. *Chemical Engineering Journal, 485*, Article 149652. https://doi.org/10.1016/j.cej.2024.149652

Tian, M., von Dahl, C. C., Liu, P.-P., Friso, G., van Wijk, K. J., & Klessig, D. F. (2012). The combined use of photoaffinity labeling and surface plasmon resonance-based technology identifies multiple salicylic acid-binding proteins. *The Plant Journal, 72*(6), 1027–1038. https://doi.org/10.1111/tpj.12016

Wang, J., Allan, A. C., Wang, W.-Q., & Yin, X.-R. (2022). The effects of salicylic acid on quality control of horticultural commodities. *New Zealand Journal of Crop and Horticultural Science, 50*(2), 99–117. https://doi.org/10.1080/01140671.2022.2037672

Wang, Y., Wang, Y., Yu, L., Wang, J., Du, B., & Zhang, X. (2019). Enhanced catalytic activity of templated-double perovskite with 3D network structure for salicylic acid degradation under microwave irradiation: Insight into the catalytic mechanism. *Chemical Engineering Journal, 368*, 115–128. https://doi.org/10.1016/j.cej.2019.02.174

Xiong, J.-F., Luo, S.-H., Huo, J.-P., Liu, J.-Y., Chen, S.-X., & Wang, Z.-Y. (2014). Design, synthesis, and characterization of 1,3,5-tri(1*H*-benzo[*d*]imidazol-2-yl)benzene-based fluorescent supramolecular columnar liquid crystals with a broad mesomorphic range. *The Journal of Organic Chemistry, 79*(17), 8366–8373. https://doi.org/10.1021/jo5016954

Yang, W., Kang, J., Liu, Y., Guo, M., & Chen, G. (2022). Effect of salicylic acid treatment on antioxidant capacity and endogenous hormones in winter jujube during shelf life. *Food Chemistry, 397*, 133788–133798. https://doi.org/10.1016/j.foodchem.2022.133788

Zeng, S., Liu, X., Kafuti, Y. S., Kim, H., Wang, J., Peng, X., … Yoon, J. (2023). Fluorescent dyes based on rhodamine derivatives for bioimaging and therapeutics: Recent progress, challenges, and prospects. *Chemical Society Reviews, 52*, 5607–5651. https://doi.org/10.1039/D2CS00799A

Zhang, H., Xiao, P., Wong, Y., Shen, W., Chhabra, M., Peltier, R., … Sun, H. (2017). Construction of an alkaline phosphatase-specific two-photon probe and its imaging application in living cells and tissues. *Biomaterials, 140*, 220–229. https://www.sciencedirect.com/science/article/pii/S0142961217304325.

Zhang, L., Chen, J., Lu, L., Yu, R., & Zhang, D. (2023). A smartphone-assisted colorimetric aptasensor based on aptamer and gold nanoparticles for visual, fast and sensitive detection of ZEN in maize. *Food Chemistry: X, 19*, Article 100792. https://doi.org/10.1016/j.fochx.2023.100792

Zhang, M., Chen, Z., Liu, X., Song, C., Zeng, C., Lv, T., Xu, Z., Chen, X., Wang, L., Liu, B., & Peng, X. (2023). Dual-mode supramolecular fluorescent probe for rapid and on-site detection of chlorpyrifos in the environment. *Journal of Hazardous Materials, 452*, Article 131177. https://doi.org/10.1016/j.jhazmat.2023.131177

Zhang, Q., Zhu, J., Wang, Y., Feng, J., Yan, W., & Xu, H. (2014). Electrochemical assisted photocatalytic degradation of salicylic acid with highly ordered TiO_2 nanotube electrodes. *Applied Surface Science, 308*, 161–169. https://doi.org/10.1016/j.apsusc.2014.04.125

Zheng, G., Li, Z., Duan, Q., Cheng, K., He, Y., Huang, S., … Sun, H. (2020). Two quenching groups are better than one: A robust strategy for constructing HOCl fluorescent probe with minimized background fluorescence and ultra-high sensitivity and its application of HOCl imaging in living cells and tissues. *Sensors and Actuators B: Chemical, 310*, 127890. https://www.sciencedirect.com/science/article/pii/S0925400520302379#fig0045.